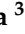*Article*

Effects of Oxygen Partial Pressure and Substrate Temperature on the Structure and Morphology of Sc and Y Co-Doped ZrO₂ Solid Electrolyte Thin Films Prepared via Pulsed Laser Deposition

Jennet R. Rabo [1], Makoto Takayanagi [2], Takashi Tsuchiya [2], Hideki Nakajima [3], Kazuya Terabe [2] and Rinlee Butch M. Cervera [1,*]

[1] Energy Storage and Conversion Materials Laboratory, Department of Mining, Metallurgical and Materials Engineering, University of the Philippines Diliman, Quezon City 1101, Philippines; jrrabo@up.edu.ph

[2] International Center for Materials Nanoarchitectonics (WIPI-MANA), National Institute for Materials Science, Tsukuba 305-0044, Ibaraki Prefecture, Japan; TAKAYANAGI.Makoto@nims.go.jp (M.T.); TSUCHIYA.Takashi@nims.go.jp (T.T.); TERABE.Kazuya@nims.go.jp (K.T.)

[3] Synchrotron Light Research Institute, Nakhon Ratchasima 30000, Thailand; hideki@slri.or.th

*   Correspondence: rmcervera@up.edu.ph; Tel.: +66-(632)-8981-8500 (ext. 3169)

Abstract: Scandium (Sc) and yttrium (Y) co-doped ZrO₂ (ScYSZ) thin films were prepared on a SiO₂-Si substrate via pulsed laser deposition (PLD) method. In order to obtain good quality thin films with the desired microstructure, various oxygen partial pressures (P_{O_2}) from 0.01 Pa to 10 Pa and substrate temperatures (T_s) from 25 °C to 800 °C were investigated. X-ray diffraction (XRD) patterns results showed that amorphous ScYSZ thin films were formed at room substrate temperature while cubic polycrystalline thin films were obtained at higher substrate temperatures (T_s = 200 °C, 400 °C, 600 °C, 800 °C). Raman spectra revealed a distinct Raman shift at around 600 cm⁻¹ supporting a cubic phase. However, a transition from cubic to tetragonal phase can be observed with increasing oxygen partial pressure. Photoemission spectroscopy (PES) spectra suggested supporting analysis that more oxygen vacancies in the lattice can be observed for samples deposited at lower oxygen partial pressures resulting in a cubic structure with higher dopant cation binding energies as compared to the tetragonal structure observed at higher oxygen partial pressure. On the other hand, dense morphologies can be obtained at lower P_{O_2} (0.01 Pa and 0.1 Pa) while more porous morphologies can be obtained at higher P_{O_2} (1.0 Pa and 10 Pa).

Keywords: co-doped zirconia; zirconia-doped thin films; pulsed laser deposition; solid electrolyte; XPS

1. Introduction

Zirconia-based solid oxide electrolyte is one of the most widely used solid electrolytes for solid oxide electrochemical cells (SOEC). It is typically doped with a trivalent cation such as yttrium to create oxygen vacancies and to stabilize the cubic structure. Yttria-stabilized zirconia (YSZ) is the typical zirconia-based solid electrolyte used for SOECs due to its high oxide ion conductivity at elevated temperatures [1–4]. Scandia-stabilized zirconia (ScSZ), on the other hand, is also used as a solid electrolyte due to its remarkable higher ionic conductivity, almost 3x, as compared to YSZ; however, the high conductivity of the cubic phase ScSZ is limited to a narrow temperature range and with the cubic phase structural stability dependent on doping concentration and temperature [5–8]. In order to circumvent these concerns and to improve the solid electrolyte properties and performance, fabrication into thin films and co-doping are some of the promising solutions.

Co-doping of scandium and yttrium into zirconia (ScYSZ) has been reported in the literature [8–13]. The incorporation of Y³⁺ and Sc³⁺ as co-dopants into ZrO₂ structure can either stabilize the cubic/tetragonal phase to achieve a better or desired property

such as higher conductivity as compared to single doping [8–11] and can provide good mechanical and thermal stability desirable for certain applications [14]. On the other hand, the fabrication of solid electrolytes into thin films may further increase the conductivity and is crucial for the development of a micron-sized SOEC system (μ-SOEC). ScYSZ thin film showed higher ionic conductivity (1.2×10^{-1}) at 700 °C (0.7 eV activation energy) as compared to bulk solid electrolytes [8,13,15].

Vapor phase deposition methods are very useful in developing thin films such as nanometer-scale electrode-electrolyte systems. Among these methods, pulsed laser deposition (PLD) has been used for the fabrication of electrolyte thin films with lower ohmic resistance and high-quality films with good morphological features. Such thin films can be attained by simply tuning the stoichiometry of the PLD target material and different deposition parameters [16,17]. Most papers have focused on the fabrication of YSZ [18–25] and ScSZ [6] via PLD and very limited reports on PLD deposited co-doped ScYSZ thin films.

The crystal structure, phase stability, and morphology are important factors that affect the properties such as the conductivity of solid electrolytes and other properties desirable for specific applications. Cubic YSZ has high ionic conductivity; however, its polymorph, tetragonal phase, although has lower conductivity, shows interesting high mechanical strength and hardness particularly also useful for solid oxide electrochemical cells applications [14,26–28]. For ScSZ, the reported ionic conductivity trend, high to low, is cubic > tetragonal > rhombohedral > monoclinic (with tetragonal phase), respectively [29]. In addition, ScSZ denser films were prepared also at low oxygen partial pressure using low-pressure plasma spray to achieve higher oxygen ion transport performance [30]. In the fabrication of thin films using PLD, the resulting crystal structure and morphology of the deposited thin films, which directly affect the electrical properties of the thin films, are dependent on the parameters employed during deposition [24,25]. For YSZ, deposited thin films show the evolution of microstructure from porous to dense thin films. High deposition temperature and lower oxygen partial pressure resulted in dense microstructure and less dense at increasing oxygen partial pressure. Dense microstructure thin film has high oxygen ion conductivity while porous thin films have low oxygen ion conductivity but have high protonic conductivity [25,31,32]. For scandium and yttrium co-doped zirconia or ScYSZ thin films, very limited information or none so far has been reported on the effects of PLD deposition parameters on the properties of ScYSZ solid electrolyte thin films. Hence, it is important to explore and investigate ScYSZ thin films fabricated via PLD.

In this study, in order to tailor and to provide an understanding of the quality of Sc and Y co-doped ZrO_2 thin films produced via PLD, the effects of different PLD deposition parameters such as oxygen partial pressure and substrate temperature on the crystal structure and morphology of Sc-Y co-doped ZrO_2 deposited thin films were investigated. The properties of prepared thin films were analyzed using X-ray diffraction (XRD), Raman spectroscopy, scanning electron microscopy (SEM), and Photoemission spectroscopy (PES).

2. Materials and Methods

The PLD ScYSZ target material, scandium and yttrium co-doped zirconia having a chemical composition of $Zr_{0.4}Y_{0.8}Sc_{0.8}O_{1.92}$, was prepared via solid state reaction method using ZrO_2 (5–25 nm, 97.2%, EM Futur, Castellon, Spain), Sc_2O_3 (99.9% Sigma-Aldrich, Inc., St. Louis, MO, USA), and Y_2O_3 (<50 nm, Sigma-Aldrich, Inc., St. Louis, MO, USA) powders. The as-calcined powder was pelletized using uniaxial pressing and finally sintered at 1400 °C in ambient condition and was used as target material for PLD. ScYSZ thin films were ablated, with a 30 mm distance, on Si with native SiO_2 oxide substrate using Nd^{3+}: YAG laser (LOTIS TII (LS-2137U), λ = 266 nm), Tokyo Instruments, Inc., Tokyo, Japan using laser energy of 38 J and a repetition rate of 10 Hz. The pulse duration was 10 ns, the area of the beam was 9.8×10^{-3} cm² and a plano-convex lens was used with a focal length of 400 mm. The as-deposited ScYSZ thin films were prepared and investigated using various PLD substrate temperatures (T_s = 25 °C, 200 °C, 400 °C, 600 °C, 800 °C) and oxygen partial pressures (P_{O_2} = 0.01 Pa, 0.1 Pa, 1.0 Pa, and 10 Pa).

The crystal structure of the as-deposited ScYSZ thin films was determined using Rigaku SmartLab X-ray Diffractometer (Rigaku Corporation, Tokyo, Japan). XRD analysis was performed using a 2-theta measurement (through NIMS-Namiki Foundry Facility, Tsukuba, Japan), equivalent to the grazing technique used for thin-film characterization. Scanning was obtained with CuKα (λ = 1.54 nm), resolution of 0.01, and 2θ scan range from 20° to 80° with 5°/min scan rate. To further investigate the crystal structure and polymorphs of ScYSZ thin films, JASCO NRS-5100 Laser Raman spectrometer (Jasco International Co., Ltd., Tokyo, Japan) was used. Raman shift of the as-deposited thin films was obtained with the wavenumber ranges from 100 cm^{-1} to 1200 cm^{-1} at room temperature. Field Emission-Scanning Electron Microscopy (FE-SEM) S-4800 (Hitachi High-Tech., Corp., Tokyo, Japan) was used to observe the morphological features of as-deposited ScYSZ thin films. Before the sample measurements, Pt films were sputtered on the surface of ScYSZ film for 20 s. Both the surface structure and the cross-sectional images were captured. Photoemission Spectroscopy (PES) was performed with Beamline 3.2Ua Photoelectron spectroscopy at the Synchrotron Light Research Institute, Nakhon Ratchasima, Thailand. The electron energy was analyzed by CLAM2 (Thermo VG Scientific, England, UK). The photon energy was 600 eV and the total energy resolution was about 2 eV. The base pressure was 2 $\times$ 10^{-8} Pa.

3. Results and Discussions

3.1. X-ray Diffraction Analysis

Figure 1 shows the diffraction peaks of polycrystalline as-deposited ScYSZ thin films using different deposition parameters: T_s and P_{O_2}. Figure 1a shows that at increasing deposition temperature, crystallized ScYSZ thin films were obtained. The as-deposited ScYSZ thin films at about 25 °C or room temperature (RT) is amorphous and crystallization started at 200 °C, then well-crystallized peaks can be observed from 600 °C to 800 °C. The diffraction peaks at $2\theta \approx 30°$ (111), 35° (200), 50° (220), 60° (311), 63° (222), and 75° (400) can be indexed and attributed to cubic ZrO$_2$-phase (ICSD No. 00-078-1808). This result is similar to the diffraction peaks measured for the target pellet and is observed to agree with the previous studies in [17,24,25] on YSZ thin films on SiO$_2$-Si substrate. On the other hand, the effect of oxygen partial pressure on the crystal structure of ScYSZ thin films is shown in Figure 1b. As shown in the XRD stacked patterns, similar peaks can be observed for the different oxygen partial pressures; however, more crystalline or high-intensity peaks are observable for the oxygen-deficient environment or lower oxygen partial pressure, P_{O_2} = 0.01 Pa and 0.1 Pa, as compared to higher oxygen partial pressures peak intensities.

3.2. Raman Spectroscopy

Figure 2a depicts the Raman spectra of the as-deposited ScYSZ thin films. When deposited at increasing deposition temperature, ScYSZ thin films show mostly cubic (**c**) phase with distinct Raman shift at approx. 600 cm^{-1}. On the other hand, while the XRD results revealed only cubic phases for all deposited samples, due to sensitivity of Raman spectroscopy to local structure and disordering as compared to XRD, there is an observed transition from cubic phase to tetragonal (**t**) phase for ScYSZ thin films deposited with increasing oxygen partial pressure as shown in Figure 2b.

As revealed in Figure 2b, in an oxygen-deficient environment or low oxygen partial pressures, P_{O_2} = 0.01 Pa and P_{O_2} = 0.1 Pa, only a single Raman band at around 600 cm^{-1} was observed suggesting a cubic ZrO$_2$ fluorite structure [28,33]. However, at increasing oxygen partial pressure, from P_{O_2} = 1.0 Pa to P_{O_2} = 10 Pa, Raman bands at approx. 298 cm^{-1}, 350 cm^{-1}, 630 cm^{-1} are observable which can be attributed to coupling of Zr-O′ stretching, O(O′)-Zr-O(O′) bending, and Zr-O stretching vibrational modes, respectively [10,28,34]. The observed Raman band at around 524 cm^{-1} is attributed to vibrational mode coming from the SiO$_2$ substrate which is more distinct at high oxygen partial pressures.
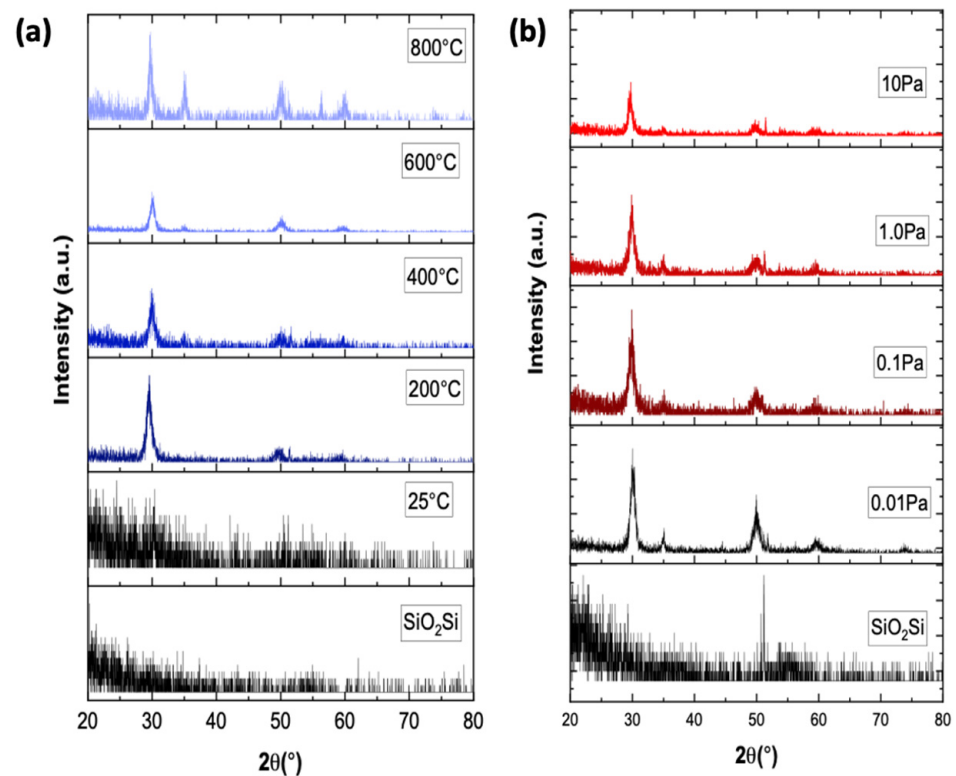
Figure 1. XRD stacked pattern. (**a**) Diffraction peaks of ScYSZ thin film on SiO_2-Si prepared with various substrate temperatures (T_s = 25 °C, 200 °C, 400 °C, 600 °C, and 800 °C) at P_{O_2} = 0.1 Pa and (**b**) XRD of ScYSZ thin film on SiO_2-Si prepared at T_s = 600 °C, with various oxygen partial pressures, P_{O_2} = 0.01 Pa, 0.1 Pa, 1.0 Pa and 10 Pa.
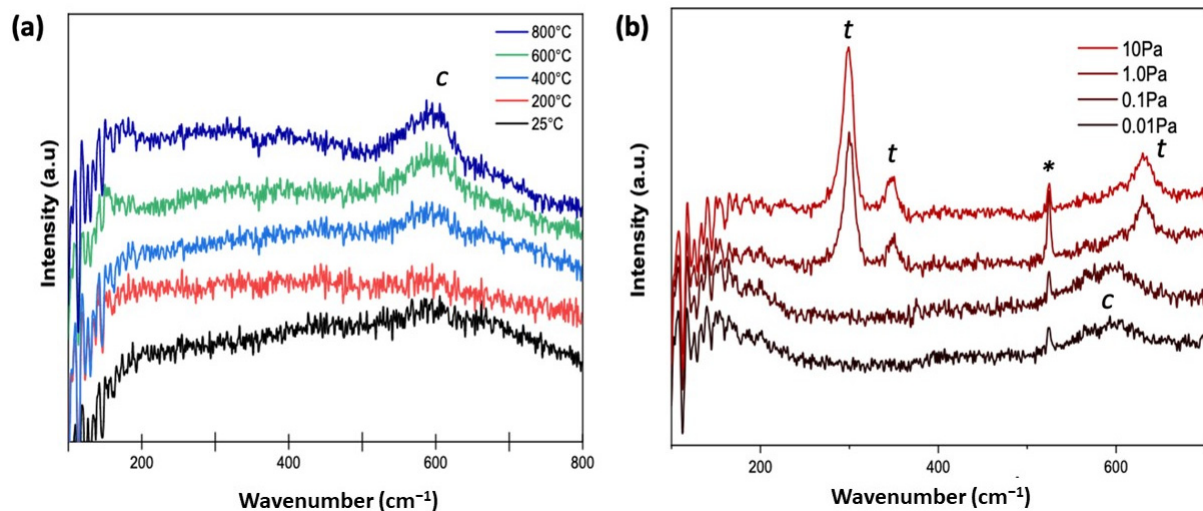

Figure 2. Raman spectra of (**a**) as-deposited ScYSZ thin films on PtTi-SiO_2-Si substrate with varying substrate deposition temperatures, T_s = 25 °C, 200 °C, 400 °C, 600 °C, and 800 °C, with constant P_{O_2} = 0.1 Pa; and (**b**) with various oxygen partial pressures, P_{O_2} = 0.01 Pa, 0.1 Pa, 1.0 Pa and 10 Pa, at T_s = 600 °C. (* SiO_2 substrate).

3.3. Microstructural Properties

Figure 3 shows the cross-sectional SEM images of the deposited thin films for T_s = 25 °C (Figure 3a) and T_s = 800 °C (Figure 3b) with oxygen partial pressure of P_{O_2} = 0.1 Pa and deposition rate of about 70 nm/h. Although both substrate temperatures showed a dense morphology, a more crystalized columnar structure can be observed at high substrate temperature.
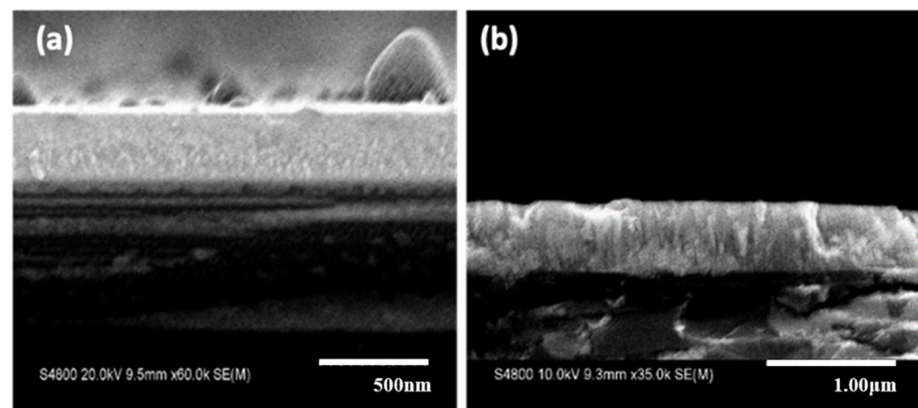
Figure 3. Cross-sectional SEM images of ScYSZ prepared at (**a**) T_s = 25 °C (**a,b**) T_s = 800 °C, with P_{O_2} = 0.1 Pa, 3 h deposition time on SiO$_2$-Si substrate.

The surface morphologies of the deposited thin films at different substrate temperatures and oxygen partial pressures are shown in Figure 4a,b, respectively. As can be observed in Figure 4a, the images revealed dense and crack-free surfaces, with the presence of droplets or circular agglomerates that increases at increasing deposition temperature. These agglomerated droplets are ScYSZ particles which are characteristic deposits for oxide films prepared using Nd:YAG laser system in PLD [20,33,35]. On the other hand, Figure 4b showed the SEM surface images of the as-deposited thin film on SiO$_2$-Si substrate at various oxygen partial pressure. At increasing oxygen partial pressure, more porous and rough surface microstructures are observable. This effect on the surface morphology using higher oxygen partial pressure during deposition is consistent with reported works on the microstructure of ZrO$_2$ thin films [19,24,25,36].

3.4. Photoemission Spectroscopy (PES)

The co-doping of Sc and Y in ZrO$_2$ and its effect on the resulting thin film structure was verified by the presence of the element's core levels and with binding energies using PES analysis [37–39] and the results are shown in Figure 5. Figure 5a shows the wide scan spectra for ScYSZ thin films deposited with P_{O_2} = 0.01 Pa and P_{O_2} = 1.0 Pa with binding energies and peaks identified for O 1s, Sc 2p, Zr 3p and Zr 3d, Y 3p and Y 3d, and O$_{KLL}$ core levels. The binding energy of the spectra was referenced from C 1s at 284.6 eV. PES peaks position for Zr 3d is at 181 eV to 183 eV which corresponds to the Zr^{4+} valence state. On the other hand, for Y 3d, the peak position is at around 158 eV for Y^{3+} valence state [40,41] and the peaks for Sc 2p are at around 402 eV to 403 eV for the Sc^{3+} valence states [38,42]. For the O 1s core levels, the peaks are expected at binding energies around 530 eV to 532 eV for lattice oxygen and hydroxyl [39], respectively, and O KLL is expected at 92 eV. The narrow scans for different core levels are shown in Figure 5b–e.

Figure 5b shows the PES stacked spectra of the O 1s core level for ScYSZ thin films deposited at P_{O_2} = 0.01 Pa and P_{O_2} = 1.0 Pa. The PES spectrum was observed to be slightly asymmetric for both P_{O_2}, 0.01 Pa and 1.0 Pa. A sample deconvolution of the peaks, for the 0.01 Pa spectrum, is also shown. As revealed, O 1s can be deconvoluted or fitted into three peaks centered at 530.0, 531.5, and 532.5 eV, for both P_{O_2}. These binding energies are typical values for O1s lattice oxygen (oxygen bonded with Zr and/or Sc/Y), hydroxyl, and weakly adsorbed oxygen/H$_2$O [42–45]. The PES stacked spectra of Zr 3d, Y 3d, and Sc 2p for the two oxygen partial pressures are shown in Figure 5c–e, respectively. Spin-orbit splitting can be observed from these spectra. Figure 5c shows the PES spectra of Zr 3d consisting of Zr 3d$_{5/2}$ and Zr 3d$_{3/2}$, corresponding to the Zr^{4+} valence state, with binding energies located at 182.4 eV and 184.8 eV for P_{O_2} = 1.0 Pa, respectively. On the other hand, Figure 5d shows the PES spectrum of Y 3d that is slightly asymmetric which consists of Y 3d$_{5/2}$ and Y 3d$_{3/2}$ with binding energies located 157.2 eV and 159.2 eV for P_{O_2} = 1.0 Pa corresponding to the Y^{3+} valence state. The PES spectrum of Sc 2p consisting of Sc 2p$_{3/2}$

and Sc $2p_{1/2}$ is shown in Figure 5e, with binding energies located at 402.4 eV and 406.9 eV ($P_{O_2} = 1.0$ Pa), corresponding to Sc^{3+} valence state.
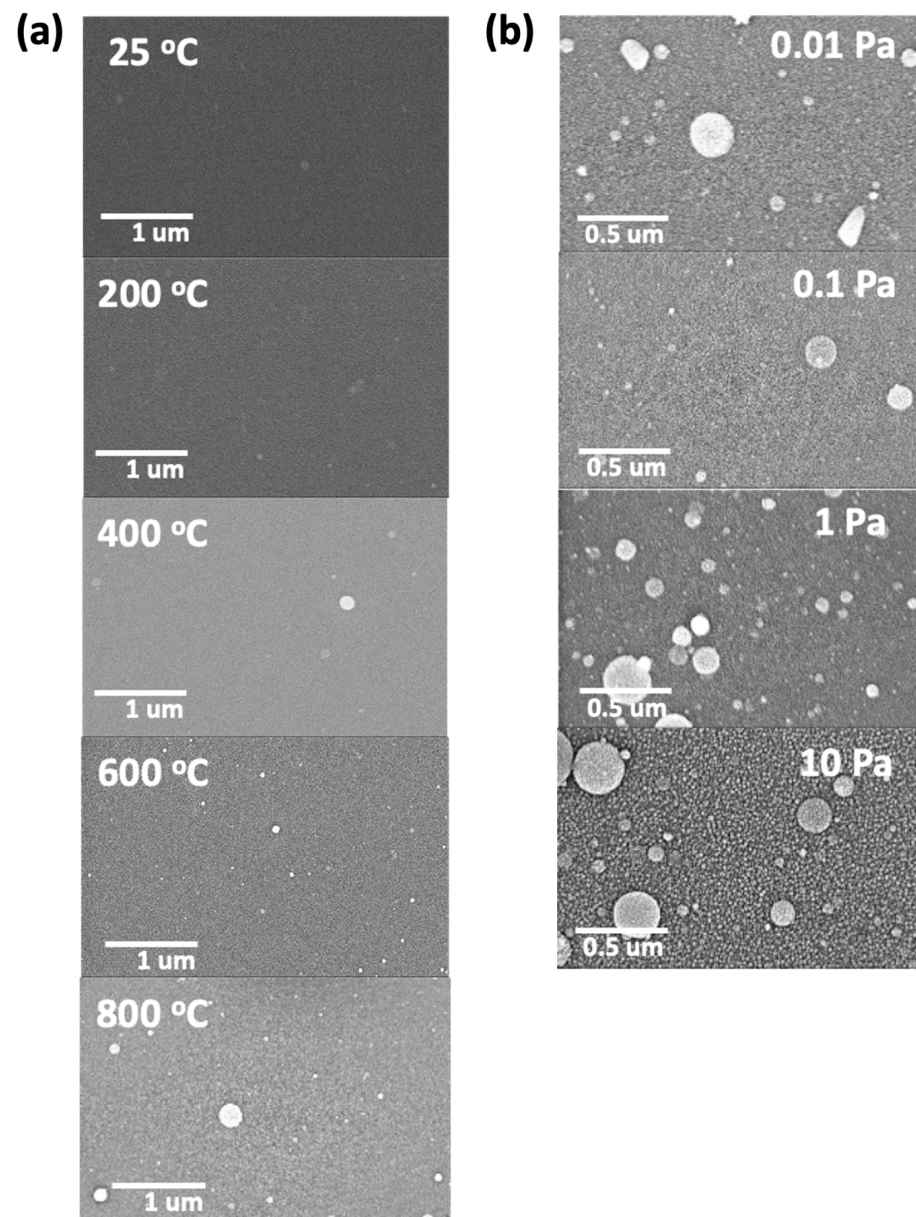

Figure 4. SEM surface morphology images of ScYSZ thin film on SiO_2-Si substrate prepared (**a**) at various substrate temperatures with constant P_{O_2} = 0.1 Pa; and (**b**) at various oxygen partial pressures (P_{O_2}) at 600 °C.

The effects of increasing P_{O_2} in the ScYSZ thin film deposition are observable by the slight shifting in the binding energies of the dopants (Y 3d/Sc 2p) core levels. The Y 3d peak shifts from 157.6 eV to 157.2 eV while Sc 2p3/2 peak shifts from 403.0 eV to 402.4 eV as oxygen pressure increases from P_{O_2} = 0.01 Pa to P_{O_2} = 1.0 Pa. This means that ScYSZ thin films deposited at P_{O_2} = 0.01 Pa suggested a higher concentration of oxygen vacancy as compared with ScYSZ thin films deposited at P_{O_2} = 1.0 Pa [39]. It can be said that the lower oxygen partial pressure induces oxygen defects or vacancies; however, as the oxygen partial pressure increases from 0.1 Pa to 1.0 Pa, the lattice oxygen increases. These suggest that the dopants were reduced when oxygen pressure was increased. On the other hand, from the results in this study, the oxygen partial pressure does not crucially affect the Zr 3d peaks. However, for the dopant cations, Y 3d and Sc 2p, the binding energy

decreases as the oxygen partial pressure increases. It can be said that at higher oxygen partial pressures, the oxygen vacancy may be filled preferentially in the vicinity of the dopant thereby significantly affecting the binding energies of Sc/Y while Zr, in general, may have no drastic changes in its environment. From the fitting data, the Zr is only slightly affected with a very small binding energy changed, about 0.02 eV difference due to the local structural change effect also with the nearest dopant. Further study is needed to support the coordination numbers of these cations and the theoretically expected formation of non-lattice oxygen with the doping that affects the binding energy. It can be said though, in this study, that the suggested presence of oxygen vacancies may be one of the reasons for the structural transition from cubic to tetragonal phase at lower to higher oxygen partial pressures, as also supported in the local structural phase transition observed from the Raman analyses.
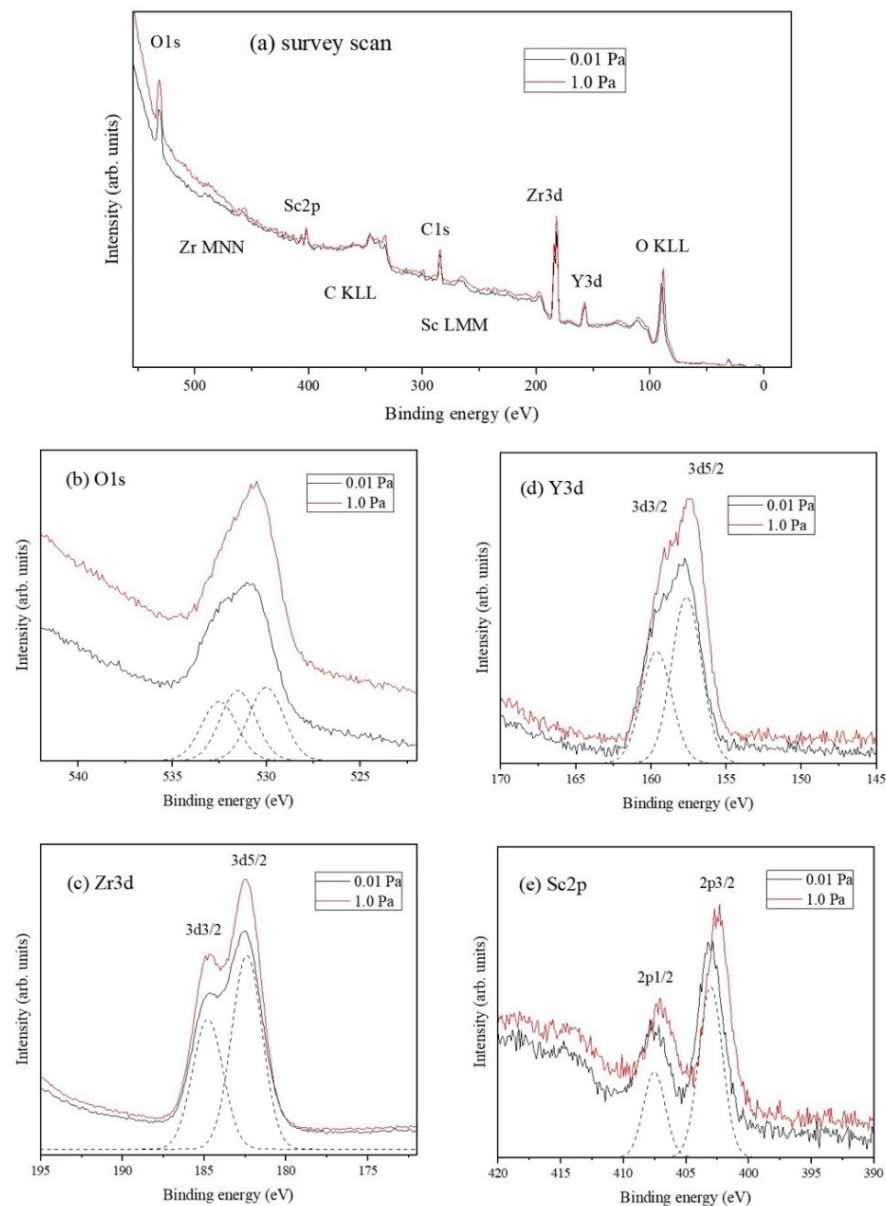

Figure 5. (**a**) PES wide scan spectra of ScYSZ thin film on SiO$_2$-Si substrate prepared at T_s = 600 °C with P_{O_2} = 0.01 Pa and P_{O_2} = 1.0 Pa, and (**b–e**) comparative stack spectra with P_{O_2} = 0.01 Pa and 1.0 Pa showing the (**b**) O 1s, (**c**) Zr 3d, (**d**) Y 3d, and (**e**) Sc 2p core levels.

4. Conclusions

Thin films of scandium and yttrium co-doped zirconia (ScYSZ) were successfully prepared on SiO_2-Si substrate using PLD under varying oxygen partial pressures (P_{O_2} = 0.01 Pa, 0.1 Pa, 1.0 Pa, and 10 Pa) and substrate temperatures (T_s = 25 °C, 200 °C, 400 °C, 600 °C, 800 °C. From the XRD analysis, an amorphous film was produced at room temperature; however, a polycrystalline cubic-phase ScYSZ can be achieved at lower oxygen partial pressures (P_{O_2} = 0.01 Pa and 0.1 Pa) and increasing substrate temperatures (T_s = 200 °C, 400 °C, 600 °C, 800 °C). The cubic structure at low oxygen partial pressure was supported by the observed Raman shifts in the Raman spectra. However, at high oxygen partial pressures (P_{O_2} = 1.0 Pa and 10 Pa), a tetragonal phase can be observed from the Raman spectra. On the other hand, SEM images revealed dense and crack-free surface morphologies with particle droplet-like agglomerates achieved at lower oxygen partial pressures (P_{O_2} = 0.01 Pa and 0.1 Pa), and rough surface and porous morphology at increasing oxygen partial pressures (P_{O_2} = 1.0 Pa and 10 Pa). Furthermore, PES spectra revealed the shifting of the dopant cations core level peaks with the increase in oxygen partial pressure from higher to lower binding energy.

References

1. Abdalla, A.M.; Hossain, S.; Azad, A.T.; Petra, P.M.I.; Begum, F.; Erickson, S.G.; Azad, A.K. Nanomaterials for solid oxide fuel cells: A review. *Renew. Sustain. Energy Rev.* **2018**, *82*, 353–368. [CrossRef]
2. Mahato, N.; Banerjee, A.; Gupta, A.; Omar, S.; Balani, K. Progress in material selection for solid oxide fuel cell technology: A review. *Prog. Mater. Sci.* **2015**, *72*, 141–337. [CrossRef]
3. Akhkozov, L.; Danilenko, I.; Podhurska, V.; Shylo, A.; Vasyliv, B.; Ostash, O.; Lyubchyk, A. Zirconia-based materials in alternative energy devices—A strategy for improving material properties by optimizing the characteristics of initial powders. *Int. J. Hydrogen Energy* **2021**, in press. [CrossRef]
4. Mansilla, Y.; Arce, M.; Oliver, G.C.; Troiani, H.; Serquis, A. Synthesis and characterization of ZrO_2 and YSZ thin films. *Mater. Today Proc.* **2019**, *14*, 92–95. [CrossRef]
5. Grosso, R.L.; Muccillo, E.N.S.; Castro, R.H.R. Enthalpies of formation in the scandia-zirconia system. *J. Am. Ceram. Soc.* **2017**, *100*, 4270–4275. [CrossRef]
6. Arachi, Y.; Sakai, H.; Yamamoto, O.; Takeda, Y.; Imanishi, N. Electrical conductivity of the ZrO_2-Ln_2O_3 (Ln = lanthanides) system. *Solid State Ion.* **1991**, *121*, 133–139. [CrossRef]
7. Garcia, R.M.; Cervera, R.B. Morphology and Structure of Ni/$Zr_{0.84}Sc_{0.16}O_{1.92}$ electrode material synthesized via glycine-nitrate combustion method for solid oxide electrochemical cell. *Appl. Sci.* **2019**, *9*, 264. [CrossRef]
8. Villanueva, M.B.; Garcia, M.R.G.; Cervera, R.B. Synthesis and characterization of Sc and Y co-doped zirconia ($Zr_{0.84}Y_{0.08}Sc_{0.08}O_{1.92}$) electrolyte prepared by sol-gel method. *Int. J. Mater. Sci. Eng.* **2018**, *6*, 99–105. [CrossRef]

9. Leoni, M.; Jones, R.L.; Scardi, P. Phase stability of scandia-yttria-stabilized zirconia TBCs. *Surf. Coat. Technol.* **1998**, *108*, 107–113. [CrossRef]

10. Borik, M.A.; Bredikhin, S.I.; Bublik, V.T.; Kulebyakin, A.V.; Kuritsyna, I.E.; Lomonova, E.E.; Milovich, P.O.; Myzina, V.A.; Osiko, V.V.; Ryabochkina, P.A.; et al. Structure and conductivity of yttria and scandia-doped zirconia crystals grown by skull melting. *J. Am. Ceram. Soc.* **2017**, *100*, 5536–5547. [CrossRef]

11. Xue, Q.N.; Wang, L.G.; Huang, X.W.; Zhang, J.X.; Zhang, H. Influence of co-doping on the conductivity of Sc-doped zirconia by first principles calculations and experiments. *Mater. Des.* **2018**, *160*, 131–137. [CrossRef]

12. Schmidt, M.S.; Hansen, K.V.; Norrman, K.; Mogensen, M. Characterization of the Ni-ScYSZ interface in a model solid oxide fuel cell anode. *Solid State Ion.* **2008**, *179*, 2290–2298. [CrossRef]

13. Alfeche, D.M.; Cervera, R.B. Highly conducting Sc and Y co-doped ZrO_2 thin films solid electrolyte on a porous Ni/YSZ electrode prepared via simple drop-coating method. *Ceram. Int.* **2020**, *46*, 10561–10567. [CrossRef]

14. Fan, W.; Bai, Y.; Wang, Z.Z.; Che, J.W.; Wang, Y.; Tao, W.Z.; Wang, R.J.; Liang, G.Y. Effect of point defects on the thermal conductivity of Sc_2O_3- Y_2O_3 co-stabilized tetragonal ZrO_2 ceramic materials. *J. Eur. Ceram. Soc.* **2019**, *39*, 2389–2396. [CrossRef]

15. Kosacki, I.; Rouleau, C.M.; Becher, P.F.; Bentley, J.; Lowndes, D.H. Nanoscale effects on the ionic conductivity in highly textured YSZ thin films. *Solid State Ion.* **2005**, *176*, 1319–1326. [CrossRef]

16. Schlupp, M.V.F.; Scherrer, B.; Ma, H.; Grolig, J.G.; Martynczuk, J.; Prestat, M.; Gauckler, L.J. Influence of microstructure on the cross-plane oxygen ion conductivity of yttria-stabilized zirconia thin films. *Phys. Status. Solidi A* **2012**, *209*, 1414–1422. [CrossRef]

17. Heiroth, S.; Lippert, T.; Wokuan, A.; Dobeli, M. Microstructure and electrical conductivity of YSZ thin films prepared by pulsed laser deposition. *Appl. Phys. A.* **2008**, *93*, 639–643. [CrossRef]

18. Reolon, R.P.; Sanna, S.; Xu, Y.; Lee, I.; Bergmann, C.P.; Pryds, N.; Esposito, V. Effects of accelerated degradation on metal supported thin film-based solid oxide fuel cells. *J. Mater. Chem. A* **2018**, *6*, 7887. [CrossRef]

19. Heiroth, S.; Frison, R.; Rupp, J.L.M.; Lippert, T.; Barthazy Meier, E.J.; Gubler, E.M.; Dobeli, M.; Conder, K.; Wokuan, A.; Gauckler, L.J. Crystallization and grain growth characteristics of yttria-stabilized zirconia thin films grown by pulsed laser deposition. *Solid State Ion.* **2011**, *191*, 12–23. [CrossRef]

20. Heiroth, S.; Lippert, T.; Wokaun, A.; Dobeli, M.; Rupp, J.L.M.; Scherrer, B.; Gauckler, L.J. Yttria-stabilized zirconia thin films by pulsed laser deposition: Microstructural and compositional control. *J. Eur. Ceram. Soc.* **2010**, *30*, 489–495. [CrossRef]

21. Ishigaki, H.; Yamada, T.; Wakiya, N.; Shinozaki, K.; Mizutani, N. Effect of the thickness of SiO_2 under layer on the initial stage of epitaxial growth process of yttria-stabilized zirconia (YSZ) thin film deposited on Si(100) substrate. *J. Ceram. Soc. Jpn.* **2001**, *109*, 766–780. [CrossRef]

22. Dubbink, D.; Koster, D.G.; Rijnders, G. Growth mechanism of epitaxial YSZ on Si by pulsed laser deposition. *Nat. Sci. Rep.* **2018**, *8*, 5774. [CrossRef] [PubMed]

23. de Coux, P.; Bachelet, R.; Gatel, C.; Warot-Fonrose, B.; Fontcuberta, J.; Sanchez, F. Mechanism of epitaxy and defects at the interface in ultrathin YSZ films on Si(001). *CrystEngComm* **2012**, *14*, 7851–7855. [CrossRef]

24. Infortuna, A.; Harvey, A.S.; Gauckler, L.J. Microstructures of CGO and YSZ thin films by pulsed laser deposition. *Adv. Funct. Mater.* **2008**, *18*, 127–135. [CrossRef]

25. Scherrer, B.; Schupp, M.V.K.; Stender, D.; Martynczuk, J.; Grolig, J.G.; Ma, H.; Kocher, P.; Lippert, T.; Prestat, M.; Gauckler, L.J. On proton conductivity in porous and dense yttria stabilized zirconia at low temperature. *Adv. Func. Mater.* **2013**, *23*, 1957–1964. [CrossRef]

26. Yashima, M.S.; Sasaki, M.; Kakihana, M.; Yamaguchi, Y.; Arashi, H.; Yoshimura, M. Oxygen-induced structural change of the tetragonal phase around the tetragonal-cubic phase boundary in ZrO_2-$YO_{1.5}$ Solid Solutions. *Acta Cryst.* **1994**, *50*, 663–672. [CrossRef]

27. Zhou, Y.; Lei, T.C.; Sakuma, T. Diffusionless cubic-to-tetragonal phase transition and microstructural evolution in sintered zirconia- yttria ceramics. *J. Am. Ceram. Soc.* **1991**, *74*, 633. [CrossRef]

28. Hwang, K.-J.; Shin, M.; Lee, M.-H.; Lee, H.; Oh, M.Y. Investigation on the phase stability of yttria-stabilized zirconia electrolytes for high-temperature electrochemical application. *Ceram. Int.* **2019**, *45*, 9462–9467. [CrossRef]

29. Huang, H.; Hsieh, C.-H.; Kim, N.; Stebbins, J.; Prinz, F. Structure, local environment, and ionic conduction in scandia stabilized zirconia. *Solid State Ion.* **2008**, *197*, 1442–1445. [CrossRef]

30. Yuan, K.; Song, C.; Chen, G.; Xu, Z.; Peng, H.; Lu, C.; Lu, X.; Ji, C. Preparation of dense thin films by plasma spraying with densified SzSC powders. *Int. J. Hydrogen Energy* **2021**, *46*, 9749–9757. [CrossRef]

31. Marcomini, R.F.; De Souza, D. Microstructural and Electrical Features of Yttrium Stabilised Zirconia with ZnO as Sintering Additive. *Mater. Res.* **2016**, *19*, 45–50. [CrossRef]

32. Ramos, C.M.; Tabata, A.S.; Cesar, P.F.; Rubo, J.H.; Francisconi, P.; Borges, A. Application of Micro-Raman Spectroscopy to the Study of Yttria-Stabilized Tetragonal Zirconia Polycrystal (Y-TZP) Phase Transformation. *Appl. Spectrosc.* **2015**, *69*, 810–814. [CrossRef]

33. Etoh, D.; Tsuchiya, T.; Takayanagi, M.; Higuchi, T.; Terabe, K. Oxide ion and proton conduction controlled in nano-grained yttria stabilized ZrO_2 thin films prepared by pulsed laser deposition. *Jpn. J. Appl. Phys.* **2019**, *58*, SDDG01. [CrossRef]

34. Takayanagi, M.; Tsuchiya, T.; Kawamura, K.; Minohara, M.; Horiba, K.; Kumigashira, H.; Higuchi, T. Proton conduction on YSZ electrolyte thin films prepared by RF magnetron sputtering. *Solid State Ion.* **2017**, *311*, 46–51. [CrossRef]

35. Chaluvadi, S.K.; Mondal, D.; Bigi, C.; Knez, D.; Rajak, P.; Ciancio, R.; Fujii, J.; Panaccione, G.; Vobornik, I.; Orgiani, P. Pulsed laser deposition of oxide and metallic thin films by means of Nd: YAG laser source operating its 1st harmonics: Recent approaches and advances. *J. Phys. Mater.* **2021**, *4*, 032001. [CrossRef]

36. Rabo, J.; Cervera, R.B.M. Fabrication of solid oxide electrolysis single cell using NiO/YSZ/YSZ/LSM-YSZ vis drop coating method. *Key Eng. Mater.* **2020**, *847*, 129–134. [CrossRef]

37. Gotsch, T.; Wallisch, W.; Stoger-Pollach, M.; Klotzer, B.; Penner, S. From zirconia to yttria: Sampling the YSZ phase diagram using sputtered-deposited thin films. *AIP Adv.* **2016**, *6*, 025119. [CrossRef]

38. Kainbayeb, N.; Sriubas, M.; Bockute, K.; Virbukas, D.; Kaukaitis, G. E-beam deposition of scandia-stabilized zirconia (ScSZ) thin films co-doped with Al. *Coatings* **2020**, *10*, 870. [CrossRef]

39. Lackner, P.; Zhou, Z.; Mayr, S.; Diebold, U.; Schmid, M. Using photoelectron spectroscopy to observe oxygen spillover to zirconia. *Phys. Chem. Chem. Phys.* **2019**, *21*, 17613. [CrossRef] [PubMed]

40. Sayan, S.; Bartynski, R.A.; Zhao, X.; Gusev, E.P.; Vanderbilt, D.; Croft, M.; Banaszak Holl, M.; Garfunkel, E. Valence and conduction band offsets of a $ZrO_2/SiO_xN_y/n$-Si CMOS gate stack: A combined photoemission and inverse photoemission study. *Phys. Stat. Sol. B* **2004**, *241*, 2246–2252. [CrossRef]

41. Sinhamahapatra, A.; Jeon, J.-P.; Kang, J.; Han, B.; Yu, J.-S. Oxygen deficient zirconia (ZrO_{2-x}): A new material for solar light absorption. *Nat. Sci. Rep.* **2016**, *6*, 27218. [CrossRef] [PubMed]

42. Dupin, J.C.; Gonbeau, D.; Vinatier, P.; Lebasseur, A. Systematic XPS studies of metal oxides, hydroxides and peroxides. *Phys. Chem. Chem. Phys.* **2000**, *2*, 1319–1324. [CrossRef]

43. Haubner, K.; Morawski, J.; Olk, P.; Eng, L.; Ziegleer, C.; Adolphi, B.; Jaehne, E. The Route to Functional Graphene Oxide. *ChemPhysChem* **2010**, *1*, 2131–2139. [CrossRef] [PubMed]

44. Takayanagi, M.; Tsuchiya, T.; Minohara, M.; Kobayashi, M.; Horiba, K.; Kumigashira, H.; Higuchi, T. Surface electronic structure of proton-doped YSZ thin film by soft-X-ray photoemission spectroscopy. *Trans. Mater. Res. Soc. Jpn.* **2017**, *42*, 61–64. [CrossRef]

45. Azdad, Z.; Marot, L.; Moser, L.; Steiner, R.; Meyer, E. Valence band behavior of zirconium oxide, photoelectron and Auger spectroscopy study. *Sci. Rep.* **2018**, *8*, 16251. [CrossRef] [PubMed]